Evaluation of the Extent of Interaction within Dimeric Tetrathiafulvalenes (TTF) Incorporating Organometallic –Hg–, –$SiMe_2$–, and –PPh– Links

Marc Fourmigué* and Yong-Sheng Huang

Laboratoire de Physique des Solides associé au CNRS, Université Paris-Sud, F-91405 Orsay, France

Received September 21, 1992

The synthesis and electrochemical properties of several organometallic tetrathiafulvalene (TTF) dimers, whose redox units are held across –Hg–, –$SiMe_2$–, or –PPh– links, are described. The extent of interaction between the TTF's in each dimer has been evaluated by cyclic voltammetry experiments and extended Hückel calculations. It appears to depend mainly on the nature of the bridging atom and the distances between the two redox centers. $(TTF)_2SiMe_2$ crystallizes in the orthorhombic system, space group *Pnma*, with a = 12.584(1) Å, b = 24.96(1) Å, c = 6.404(1) Å, and Z = 4.

Introduction

Tetrathiafulvalenes (TTF's) are widely used as π-electron donors for the formation of highly conducting charge-transfer or binary cation-radical salts.[1–4] It has been recently postulated[5] that those dimeric TTF's whose redox moieties are covalently attached could be appropriate candidates for suppressing the Peierls instabilities[6] characteristic of one-dimensional conducting systems.

Several organic- ($-(CH_2)_n-$, –Ar–, $-S(CH_2)_nS-$)[7–9] and chalcogen-linked (S, Se, Te)[10,11] TTF dimers have already been described, and tertiary "redox" phosphines[12] $(TTF)_nPh_{3-n}P$ (n = 1–3) were recently synthesized. However, systematic studies on the extent of interaction between the two redox moieties are lacking. To that end, one has to distinguish between short monoatomic spacers such as a $-CH_2-$ or a chalcogen atom, where the interactions between the redox moieties are controlled by the quite rigid geometry of the molecule, and longer spacers with an increased number of degrees of freedom, which will allow the molecule to fold and the two TTF moieties to stack on top of each other upon oxidation. The latter effect was actually postulated by Jørgensen et al. for a trimethyltetrathiafulvalene dimer with a $-S(CH_2)_nS-$ (n = 1, 2) link.[8b] Note also that in the case where the redox moieties are coupled directly, as in the bis-TTF[7b] or its trimethyl-substituted analog,[9] no interaction was observed by electrochemistry since the two redox groups are, unexpectedly, oxidized at a single potential. Clearly, a careful investigation of these intramolecular interactions is needed and *monoatomic* links appear particularly well suited for exploring the diversity of possible interactions. The latter are expected to be sensitive to the geometrical arrangement around the linking atom as well as upon its very nature (orbital energy, hybridization, presence of lone pairs). Thus, if the two redox moieties are linked across *main-group* elements, a large variety of situations may occur, ranging from linear links for mercury to tetrahedral silicon (–$SiMe_2$–), phosphorus (–PPh–), or chalcogen links, with zero, one, or two lone pairs, respectively.

Also, similar dimeric compound involving two ferrocene redox moieties have been the subject of intense work, primarily concerned with the properties of mixed-valence monooxidized salts, and fruitful comparisons with our TTF analogs can be established. Also, while numerous oxidized dimeric ferrocenes have been reported, cation radical salts of analogous TTF dimers have not been explored so far and are of interest for their electrical, magnetical, and optical properties.

In the present paper, we report on our recent work concerning –Hg–, –$SiMe_2$–, or –PPh– linked TTF dimers. The synthetic method established for TTF itself has been extended to 3,4-dimethyltetrathiafulvalene (o-DMTTF) and trimethyltetrathiafulvalene (tMTTF), allowing for variations in the donor character (o-DMTTF, tMTTF) as well as the steric bulk (tMTTF) of the two redox moieties (Chart I). The molecular structure of $(TTF)_2SiMe_2$ has been obtained from a single-crystal X-ray structure determination. The extent of interaction between the two redox units in all these dimers has been inferred from cyclic voltammetry experiments and extended Hückel calculations and compared with that of some other TTF dimers as well as analogous ferrocene compounds.

Results and Discussion

Synthesis and X-ray Structure Determination. Possibly the most general method for the synthesis of

(1) For recent advances in this field, see for example the Proceedings of the International Conference on Synthetic Metals in: *Synth. Met.* **1991**, 41–43.
(2) Wudl, F. *Acc. Chem. Res.* **1984**, *17*, 227.
(3) Torrance, J. B. In *Low Dimensional Conducts and Superconductors*; Jerome, D., Caron, L. G., Eds.; NATO ASI Series 155; Plenum: New York, 1987; p 113.
(4) Whango, M. H. *Acc. Chem. Rev.* **1983**, *16*, 95.
(5) Bechgaard, K.; Lerstrup, K.; Jørgensen, M.; Johannsen, I.; Christensen, J. In *The Physics and Chemistry of Organic Superconductors*; Saito, G., Kagoshima, S., Eds.; Springer-Verlag: Berlin, 1990; p 349.
(6) However, as pointed out by one of the reviewers, in one-dimensional two-band systems, interband nesting can open a band gap in the two bands: (a) Pouget, J. P.; Noguera, C.; Moudden, A. H.; Moret, R., *J. Phys. (Les Ulis, Fr.)* **1985**, *46*, 1731. (b) Canadell, E.; Whangbo, M. H. *Chem. Rev.* **1991**, *91*, 965.
(7) (a) Kaplan, M. L.; Haddon, R. C.; Wudl, F. *J. Chem. Soc., Chem. Commun.* **1977**, 388. (b) Iyoda, M.; Kuwatani, Y.; Ueno, N.; Oda, M. *J. Chem. Soc., Chem. Commun.* **1992**, 158.
(8) (a) Adam, M.; Wolf, P.; Räder, H.-J.; Müllen, K. *J. Chem. Soc., Chem. Commun.* **1990**, 1624. (b) Jørgensen, M.; Lerstrup, K.; Bechgaard, K. *J. Org. Chem.* **1991**, *56*, 5684.
(9) Bechgaard, K.; Lerstrup, K.; Jørgensen, M.; Johanssen, I.; Christensen, J. In ref 5, p 383.
(10) Becker, J. Y.; Bernstein, J.; Bittner, S.; Sarma, J. A. R. P.; Shahal, L. *Tetrahedron Lett.* **1988**, *29*, 6177.
(11) Bryce, M. R.; Cooke, G.; Dhindsa, A. S.; Ando, D. J.; Hursthouse, M. B. *Tetrahedron Lett.* **1992**, *33*, 1783.
(12) Fourmigué, M.; Batail, P. *Bull. Soc. Chim. Fr.* **1992**, *129*, 29.

0276-7333/93/2312-0797$04.00/0

Chart I

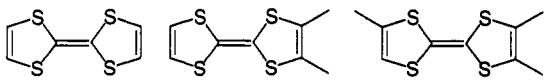

Scheme I

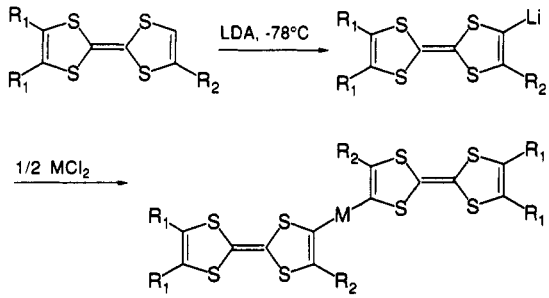

	$R_1=R_2=H$ TTF	R_1=Me, R_2=H o-DMTTF	$R_1=R_2$=Me tMTTF
M=-Hg-	1a	1b	1c
M=-$SiMe_2$-	2a	2b	2c
M=-PPh-	3a	3b	3c

σ-bonded organometallic compounds is the reaction of an organolithium or Grignard reagent with a halide derivative of the metal or main-group element. This reaction has been successfully applied to TTF-Li, affording its functionalization with various organometallic substituents.[7b,10-13] Thus, treating 2 equiv of tetrathiafulvalenyllithium[14] at −70 °C in Et_2O with $HgCl_2$, Me_2SiCl_2, or $PhPCl_2$ leads to the dimeric compounds **1a** (-Hg-), **2a** (-$SiMe_2$-), and **3a** (-PPh-) (Scheme I). While **2a** and **3a** are as soluble as TTF in all common solvents, the Hg derivative **1a** could only be dissolved in strongly coordinating solvents such as DMF, DMSO, and pyridine, from which it can be recrystallized, albeit with extensive decomposition at the highest temperatures. An improved stability of the mercuric dimers was expected with the methylated TTF's o-DMTTF and tMTTF, whose synthesis has been recently described.[15] Thus, for example, reacting tMTTF with lithium diisopropylamide (LDA) in Et_2O at low temperature leads to the formation of a yellow precipitate of the lithium derivative, which is then similarly derivatized with $HgCl_2$, Me_2SiCl_2, or $PhPCl_2$. Note that the hitherto reported successful lithiation of tMTTF at low temperature is of particular interest. Indeed, it is specified in Green's seminal paper on TTF-Li[14] that those protons deactivated with an adjacent methyl group failed to react with LDA at −78 °C, in contrast to the present observations. As expected, the stability of the Hg derivatives **1b** and **1c** was improved and they could be now be recrystallized from DMF as very thin yellow platelets with little degradation.

A full crystal structure determination has been conducted for **2a** in order to determine the geometry around the silicon atom and to compare it with analogous chalogen-linked dimers whose structures were recently described.[10,11] **2a** crystallizes in the orthorhombic system, space group

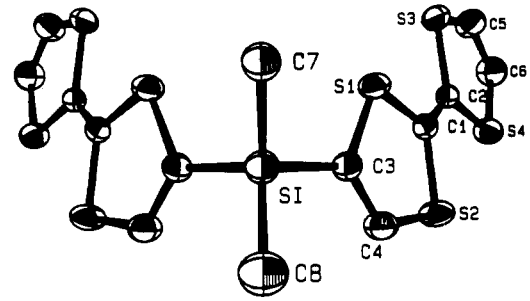

Figure 1. ORTEP drawing and numbering scheme for $(TTF)_2SiMe_2$ (**2a**). Thermal ellipsoids are drawn at the 50% probability level.

Table I. Final Positional and Equivalent Isotropic Thermal Parameters in $(TTF)_2SiMe_2$ (2a)

atom	x	y	z	B_{eqv}/Å^2
S(1)	0.79780 (9)	0.33385 (5)	0.1745 (2)	6.18 (3)
S(2)	1.0053 (1)	0.38776 (5)	0.1767 (3)	7.33 (4)
S(3)	0.7267 (1)	0.40207 (5)	−0.2322 (3)	7.03 (3)
S(4)	0.9333 (1)	0.45757 (5)	−0.2304 (3)	6.99 (3)
Si	0.8610 (2)	0.25000	0.5168 (3)	5.55 (4)
C(1)	0.8800 (3)	0.3816 (2)	0.0538 (7)	5.1 (1)
C(2)	0.8517 (3)	0.4094 (2)	−0.1120 (7)	5.1 (1)
C(3)	0.8914 (3)	0.3097 (2)	0.3514 (7)	5.2 (1)
C(4)	0.9843 (4)	0.3356 (2)	0.3497 (9)	6.4 (1)
C(5)	0.7516 (5)	0.4470 (2)	−0.424 (1)	8.6 (2)
C(6)	0.8440 (5)	0.4720 (2)	−0.427 (1)	8.5 (2)
C(7)	0.7187 (5)	0.2500	0.583 (1)	7.0 (2)
C(8)	0.9492 (7)	0.2500	0.747 (1)	8.3 (2)

Table II. Important Bond Distances (Å) and Angles (deg) in $(TTF)_2SiMe_2$ (2a)

Distances

S(1)–C(1)	1.756 (5)	S(3)–C(5)	1.692 (7)	Si–C(8)	1.842 (8)
S(1)–C(3)	1.741 (5)	S(4)–C(2)	1.753 (5)	C(1)–C(2)	1.317 (6)
S(2)–C(1)	1.768 (5)	S(4)–C(6)	1.722 (7)	C(3)–C(4)	1.335 (6)
S(2)–C(4)	1.730 (6)	Si–C(3)	1.868 (5)	C(5)–C(6)	1.320 (8)
S(3)–C(2)	1.760 (5)	Si–C(7)	1.839 (7)		

Angles

C(1)–S(1)–C(3)	97.0 (2)	S(1)–C(1)–C(2)	123.6 (4)
C(1)–S(2)–C(4)	94.7 (2)	S(2)–C(1)–C(2)	123.5 (4)
C(2)–S(3)–C(5)	94.7 (3)	S(3)–C(2)–S(4)	114.0 (3)
C(2)–S(4)–C(6)	94.4 (3)	S(3)–C(2)–C(1)	122.5 (4)
C(3)–Si–C(3)	105.9 (3)	S(4)–C(2)–C(1)	123.5 (4)
C(3)–Si–C(7)	109.2 (2)	S(1)–C(3)–Si	120.4 (3)
C(3)–Si–C(8)	109.2 (2)	S(1)–C(3)–C(4)	114.8 (4)
Si–C(3)–C(4)	124.7 (4)	S(2)–C(4)–C(3)	120.2 (4)
C(7)–Si–C(8)	113.8 (4)	S(3)–C(5)–C(6)	119.0 (5)
S(1)–C(1)–S(2)	112.9 (3)	S(4)–C(6)–C(5)	117.8 (5)

Pnma, with a = 12.584(1) Å, b = 24.96(1) Å, and c = 6.404(1) Å. Final positional and equivalent isotropic thermal parameters are given in Table I and important bond distances and angles in Table II. The molecule is located on a mirror plane (Figure 1); the coordination geometry around the Si atom is essentially tetrahedral, with C–Si–C angle values of 105.9(3), 109.2(2), and 113.85(4)°. As observed in several structures of neutral TTF derivatives,[13,16,17] the TTF moiety in **2a** presents significant deviations from planarity. It adopts a chair conformation with each dithiole ring slightly bent along the S–S axis, up to 6.6(7)° along S(1)–S(2). The two TTF moieties are not coplanar; the angle between the normals to the two TTF planes amounts to 88.92(3)°, a probable consequence

(13) Fourmiqué, M.; Batail, P. *J. Chem. Soc., Chem. Commun.* **1991**, 1370.
(14) Green, D. C. *J. Org. Chem.* **1979**, *44*, 1476.
(15) Lerstrup, K.; Johannsen, I.; Jørgensen, M. *Synth. Met.* **1988**, *27B*, 9. See also ref 8.
(16) Novoa, J. J.; Whangbo, M. H.; Williams, J. M. *Mol. Cryst. Liq. Cryst.* **1990**, *181*, 25.
(17) Whangbo, M. H.; Jung, D.; Ren, J.; Evain, M.; Novoa, J. J.; Mota, F.; Alvrez, S.; Williams, J. M.; Beno, M. A.; Kini, A. M.; Wang, H. H.; Ferraro, J. R., In ref 5, p 262.

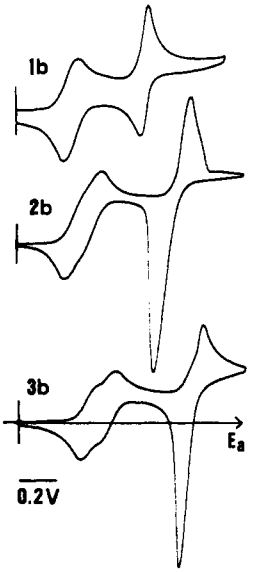

Figure 2. Cyclic voltammograms of (o-DMTTF)$_2$Hg (**1b**), (o-DMTTF)$_2$SiMe$_2$ (**2b**), and (o-DMTTF)$_2$PPh (**3b**), recorded in CH_2Cl_2 (except **1b** in DMF) at a scan rate of 100 mV/s.

Table III. Cyclic Voltammetry Data for the New Donors and the Corresponding Monomers (TTF, o-DMTTF, tMTTF) vs SCE in CH_2Cl_2 with 0.05 M nBu_4PF_6 (Scan Speed 100 mV/s)

compd	$E^1_{1/2}$ (V)	$E^2_{1/2}$ (V)
(TTF)$_2$Hg (**1a**)	0.35 (in DMF, broad)	0.68 (in DMF, broad)
(TTF)$_2$SiMe$_2$ (**2a**)	0.29, 0.38	0.77
(TTF)$_2$PPh (**3a**)	0.37, 0.47	0.84
TTF	0.32	0.72
(o-DMTTF)$_2$Hg (**1b**)	0.27 (in DMF, broad)	0.66 (in DMF, broad)
(o-DMTTF)$_2$SiMe$_2$ (**2b**)	0.22, 0.32	0.82
(o-DMTTF)$_2$PPh (**3b**)	0.28, 0.38	0.88
o-DMTTF	0.34	0.71
(tMTTF)$_2$Hg (**1c**)	0.28 (in DMF, broad)	0.63 (in DMF, broad)
(tMTTF)$_2$SiMe$_2$ (**2c**)	0.24, 0.34	0.88
(tMTTF)$_2$PPh (**3c**)	0.23, 0.36	0.76, 0.87
tMTTF	0.21	0.79

of the repulsion of the lone pairs of the sulfur atoms S(1) and S(1)′. This near-orthogonality, also observed in (TTF)$_2$S[11] and (TTF)$_2$Te,[10] may have consequences on the π-orbital interactions between the two TTF redox moieties (see below). The shortest intermolecular S---S distances exceed 3.95 Å, demonstrating that there is no sizable intermolecular interactions in **2a**, in the solid state.

Electrochemistry. Cyclic voltammetry experiments were performed for each new donor, and the results are collected in Table III together with oxidation potential references taken from literature data. First, note the electron-donating effect of a –SiMe$_2$(TTF) moiety on the adjacent TTF unit, which gives it a lower oxidation potential, compared to that of an unsubstituted TTF molecule. It contrast, an electron-withdrawing effect is observed for a –PPh(TTF) moiety, thereby resulting in its higher oxidation potential when compared to TTF. Also, as one goes from TTF to o-DMTTF and tMTTF, oxidations occur at decreasing potentials, as expected from the well-known donating ability of the methyl substituents.

Three distinct oxidation waves are observed for the silicon and phosphorus derivatives (Figure 2). These data are consistent with the sequential formation of the mono- and dicationic species, followed by a further two-electron oxidation to the tri- and tetracationic species. These features, already observed in reported TTF dimers with

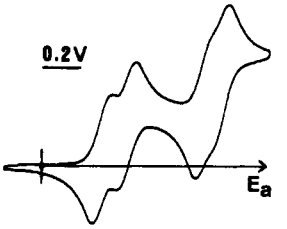

Figure 3. Cyclic voltammogram of (tMTTF)$_2$PPh (**3c**), recorded in CH_2Cl_2 at a scan rate of 100 mV/s.

organic or organometallic links,[9,11] have been ascribed to a nonnegligible interaction between the two redox moieties. Note also that the oxidation to the tri- and tetracation is found to occur at a single potential, a behavior associated with the sharpening of the corresponding reduction peak, attributable to adsorption/precipitation phenomena at the electrode.

Two classes of compounds exhibiting different types of voltammograms have been identified. For the mercury derivatives, only two broad oxidation waves are observed (Figure 2), indicating that both TTF redox fragments are oxidized at the same potential; oxidation of the first TTF does not affect the ease with which the second TTF is oxidized. Note, however, that this broadening could be ascribed, in part, to the effect of the highly polar solvent (DMF) used, where the changed species are very well screened.[18] On the other hand, in (tMTTF)$_2$PPh (**3c**) four waves are clearly seen (Figure 3). Here, for the first time and probably because of their higher solubility, sequential oxidation to the mono-, di-, tri-, and tetracations is observed.

As pointed out in the Introduction, the set of dimeric TTF's with a monoatomic link such as –S–, –CH$_2$–, –PPh–, –SiMe$_2$–, and –Hg– provides a unique opportunity to gain more insight into the extent and nature of the interactions between the two redox groups. Of particular interest is the separation between the first two oxidation waves. A strong interaction would lead to a large separation, since once it is oxidized to the monocation, the molecule will be all the more difficult to oxidize to the dication because of the delocalization of the positive charge in the monocation. Values of $\Delta E^1_{1/2}$ for a variety of such TTF dimers, taken from this work or from the literature, have been collected in Table IV, along with published data for the analogous biferrocenes. Strikingly, a very similar behavior appears for the four different donors TTF, o-DMTTF, tMTTF, and ferrocene, from the mercury link with the smallest $\Delta E^1_{1/2}$ values to the sulfur link, which presents the highest $\Delta E^1_{1/2}$ values. It follows that the linkages can be classified according to these $\Delta E^1_{1/2}$ values, in the following order: –S– > –CH$_2$–, –PPh– > –SiMe$_2$– > Hg. Note also that $\Delta E_{1/2}$ values are larger for ferrocene dimers than for TTF dimers (see below).

Discussion and Theoretical Results. The similar nature of the links presented in this paper allows for a detailed discussion of the extent and nature of the

(18) Lichtenberger, D. L.; Johnston, R. L.; Hinkelmann, K.; Suzuki, T.; Wudl, F. *J. Am. Chem. Soc.* **1990**, *112*, 3302.
(19) O'Connor, Salazar, D. L.; Cowan, D. O. *J. Organomet. Chem.* **1991**, *408*, 227.
(20) Morrison, W. H., Jr.; Krogsrud, S.; Hendrickson, D. N. *Inorg. Chem.* **1973**, *12*, 1998.
(21) Kotz, J. C.; Nivert, C. L.; Lieber, J. M.; Reed, C. D. *J. Organomet. Chem.* **1975**, *91*, 87.
(22) Bocarsly, A. B.; Walton, E. G.; Bradley, M. G.; Wrighton, M. S. *J. Electroanal. Chem. Interfacial Electrochem.* **1979**, *100*, 283.

Table IV. Oxidation Potential Difference $\Delta E^1_{1/2}$ (mV) between the First Two Oxidation Waves of TTF and Ferrocene Dimers

	TTF	o-DMTTF	tMTTF	ferrocene
–S–	$(TTF)_2S$,[a] 120			$(Fc)_2S$,[b] 290
$–CH_2–$			$(tMTTF)_2CH_2$,[c] 140	$(Fc)_2CH_2$,[d] 170
–PPh–	$(TTF)_2PPh$, 100	$(o\text{-}DMTTF)_2PPh$, 100	$(tMTTF)_2PPh$, 130	$(Fc)_2PPh$,[e] 160
$–SiMe_2–$	$(TTF)_2SiMe_2$, 90	$(o\text{-}DMTTF)_2SiMe_2$, 100	$(tMTTF)_2SiMe_2$, 100	$(Fc)_2SiMe_2$,[f] 145
–Hg–	$(TTF)_2Hg$, broad	$(o\text{-}DMTTF)_2Hg$, broad	$(tMTTF)_2Hg$, broad	$(Fc)_2Hg$,[d] 0

[a] Reference 11. [b] Reference 19. [c] Reference 9. [d] Reference 20. [e] Reference 21. [f] Reference 22.

Table V. Calculated Energy Difference between the HOMO's in the (TTF···TTF) Fragments ($\Delta E_{TTF\cdots TTF}$) and in the Whole Molecule ($\Delta E_{(TTF)_2M}$) and Observed Heteroatom–Carbon Distances and Angles in the Dimers

dimer	$\Delta E_{TTF\cdots TTF}$ (meV)	$\Delta E_{(TTF)_2M}$ (meV)	d_{M-C} (Å)	C–M–C angle (deg)
$(TTF)_2S$	34	51	1.76–1.77	100.6
$(TTF)_2PPh$	110	133	1.81–1.84	100–103
$(TTF)_2SiMe_2$	47	43	1.84–1.87	105.9
$(TTF)_2Hg$	0.5	27	2.06–2.08	180

interactions between the two electron-rich moieties upon oxidation. Two effects need to be taken into account, namely the Coulombic interactions and the molecular orbital overlap. The first effect is essentially steric and will depend on the geometry and the rigidity of the dimer; that is, how far from each other are the two redox moieties? The second effect can be divided into two contributions, namely, the through-space overlap between the two $HOMO_{TTF}$'s and a through-bond contribution which originates in the relative position, orientation, and energy of the two $HOMO_{TTF}$'s with respect to the orbitals of the linking fragment. A strong orbital interaction, either through-space and/or through-bond, will lead to a non-negligible splitting of the two degenerate HOMO's and hence will be related to a larger separation of the two oxidation steps.

In the so-called extended Hückel fragment molecular orbital (FMO) analysis,[23] the through-space contribution to the interaction can be characterized by the energy difference $\Delta E_{TTF\cdots TTF}$ between the two HOMO's of the fragment (TTF···TTF) only, in the same relative orientation as in the dimer. Interaction of these fragment orbitals with the linking-group fragment orbitals then leads to the complete orbital set of the dimeric molecule. An increase of the gap between the two HOMO's, upon interaction with the linking-group orbitals, thus will indicate a through-bond contribution to the overlap between the two frontier orbitals. The results of the calculations are collected in Table V.

As observed in several diarylmercury compounds,[24,25] the mercury atom is likely to be linearly coordinated (C–Hg–C ≈ 180°), which places the two redox moieties far apart from each other (d_{Hg-C} = 2.06–2.08 Å). In addition, the molecule is assumed to be centrosymmetrical. Under those conditions, extended Hückel calculations for $(TTF)_2Hg$ show that the two essentially degenerate HOMO's are the bonding and antibonding combinations of the $HOMO_{TTF}$. A fragment analysis, with the (TTF···TTF) orbitals on the one hand and the mercury atom orbitals on the other hand, demonstrates that the mercury orbitals are hardly involved in the final HOMO's. In fact, the perfect degeneracy of the two HOMO's of the fragment (TTF···TTF), in the constrained geometry defined above, is removed by only 0.027 eV through the interaction with the 6p Hg orbital, located 1.6 eV higher in energy.[26] Thus, with the mercury link, the two TTF redox groups can be regarded as completely isolated from each other, a conclusion reached independently from the cyclic voltammetry experiments.

In contrast, the $–SiMe_2–$, –PPh–, and –S– links impose a common tetrahedral conformation and the differences between the dimers are solely the carbon–heteroatom bond lengths and the presence of substituents or lone pairs on the bridging heteroatom. Using the geometry of $(TTF)_2S$[11] and $(TTF)_2SiMe_2$ obtained from the crystal structure determinations, a small through-space contribution to the overlap between the TTF redox moieties is found ($\Delta E_{TTF\cdots TTF}$ = 30–50 meV). For $(TTF)_2PPh$, a sound geometry was obtained from the $P(TTF)_3$ structure determination[13] by substituting one of the TTF groups with a phenyl group and running a molecular mechanics energy minimization. Due to the pyramidal shape of the phosphine and the steric demand of the phenyl ring, the two TTF moieties are closer together and, accordingly, the calculated through-space contribution $\Delta E_{TTF\cdots TTF}$ amounts to ~110 meV.

It is then of interest to analyse how $\Delta E_{TTF\cdots TTF}$ is affected when the (TTF···TTF) fragment orbitals are mixed with the orbitals of the linking fragment. This is summarized in Table V. With the $–SiMe_2–$ group, the splitting of the two HOMO's remains essentially the same. There is no contribution of the orbitals of the $–SiMe_2–$ linkage in the HOMO's of the dimer and, hence, no through-bond overlap. The situation appears somewhat different for the –PPh– and –S– links, where the splitting of the HOMO's of the fragment (TTF···TTF) slightly increases upon interaction with the lone pairs of the central fragment orbitals. However, this through-bond contribution to the overlap remains very small, of the same order of magnitude as that calculated for $(TTF)_2Hg$.

Therefore, it turns out that through-space and through-bond overlap between the two π-type $HOMO_{TTF}$'s are both negligible. The lack of through-bond coupling follows from the nature of the frontier orbital of the tetrathiafulvalene molecule. The π-type HOMO of TTF is essentially localized on the sulfur atoms and the central C=C bond, with a small contribution of the outer carbon atoms (Figure 4). The small coefficient at the branching carbon atom thus prevents any sizable through-bond overlap between the two $HOMO_{TTF}$'s and the orbitals of the linking fragment, even when these orbitals are appropriately oriented.

(23) Hoffmann, R. *J. Chem. Phys.* **1963**, *39*, 1397. Single-ζ calculations have been conducted, and the following parameters (H_{ii}) and orbital exponents (ζ) for the heteroatoms have been used. S: 3s, H_{ii} = –20.00 eV, ζ = 1.817; 3p, H_{ii} = –13.3 eV, ζ = 1.817. P: 3s, H_{ii} = –20.20 eV, ζ = 1.880; 3p, H_{ii} = –12.5 eV, ζ = 1.880. Si: 3s, H_{ii} = –17.30 eV, ζ = 1.383; 3p, H_{ii} = –9.20 eV, ζ = 1.383. Hg: 6s, H_{ii} = –13.68 eV, ζ = 2.649; 6p, H_{ii} = –8.47 eV, ζ = 2.631.

(24) Willinson, D. L.; Riede, J.; Müller, G. *Z. Natuforsch.* **1991**, *46B*, 285.

(25) Mathew, M.; Kunchur, N. R. *Can. J. Chem.* **1969**, *47*, 429.

(26) This situation was not essentially changed when the 6p Hg orbital was lowered by 1 eV. Consequently, our result is not parameter-dependent. The noncoupling of the two moieties seems to be due to the small coefficients at the outer carbon sites in the TTF HOMO and the very diffuse nature of the Hg 6p orbitals.

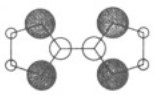

Figure 4. Atomic coefficients in the HOMO of TTF. The radii of circles are approximately proportional to the atomic coefficients.

Thus, no orbital interaction of any kind is able to account for the observed trends of $\Delta E^1_{1/2}$ within the series of dimers. It is then concluded that the dominant interaction is to be ascribed to the Coulombic charge repulsions and then will be expected to depend mainly on the separation between the two TTF's. In the linearly coordinated mercury compound, Coulombic and overlap interactions are both very weak and the two TTF's are independent. In the tetrahedral dimers, the closeness of the two TTF fragments may be evaluated by comparing the heteroatom–carbon distances (d_{M-C}) as well as the carbon–heteroatom–carbon angles (Table V). The shortest distances and smallest angles are in fact observed with the sulfur link and the largest ones with the $-SiMe_2-$ link, a trend which parallels the electrochemical data.

Similar conclusions can be drawn for the ferrocene derivatives. The HOMO of the ferrocene is mainly centered on the iron atom, with very small contributions of the cyclopentadienyl carbon atoms. Therefore, similar arguments would rule out any sizable intramolecular Fc–Fc overlap and predict that Coulombic effects will dominate the redox properties. A rationale for the larger values of $\Delta E^1_{1/2}$ in the dimeric ferrocene series, as compared to the corresponding dimeric TTF series (Table IV), is then to be found in shorter Fe–Fe distances, while the $HOMO_{TTF}$ is much more diluted over the C_2S_4 central fragment of the molecule, leading to smaller atomic charges.

Charge-Transfer and Cation-Radical Salts. Several preliminary experiments have been conducted for the elaboration of new conducting materials from these dimeric tetrathiafulvalenes, either as charge-transfer salts with electron acceptors such as TCNQ or as cation-radical salts with various closed-shell anions.

When CH_3CN solutions of **2a** or **2b** are treated with 1 equiv of tetracyanoquinodimethane (TCNQ), dark blue solutions are obtained, from which microcrystalline powders are isolated upon cooling. Compressed-pellet conductivity measurements show a semiconducting behavior for both salts with $\sigma \approx (3-5) \times 10^{-5}$ S·cm^{-1} and an activation energy of 0.6 eV. Similarly, addition of TCNQ to the DMF or PhCN solutions of the mercury derivatives **1a** and **1b** leads to the immediate apparition of dark green insoluble precipitates of the 1:1 salts **1a**·TCNQ and **1b**·TCNQ. These compounds also exhibit a semiconducting behavior with higher conductivity ($\sigma \approx 10^{-2}$ S·cm^{-1}) and lower activation energy (0.2 eV). Attempts to grow crystals by slow diffusion methods have to date been unsuccessful.

Electrocrystallization has proved a very successful method for the observation of high-purity single crystals of a variety of cation-radical salts.[27] Attempts to grow crystals by this method from the silicon derivatives result in the breaking of the carbon–silicon bond as demonstrated by the obtention of single crystals of several phases, which had already been described with TTF itself. Thus, with $(TTF)_2SiMe_2$ (**2a**) and the molybdenum halide cluster dianion $Mo_6Cl_{14}^{2-}$, crystals of the ternary salt $(TTF^+)_3(Cl^-)(Mo_6Cl_{14}^{2-})$ were obtained,[28] while with the chalcohalide cluster monoanion $Re_6S_5Cl_9^-$,[29] TTF-Cl was isolated instead as indicated by unit cell determination of the long black needles which proved identical with reported data.[30]

A contrasting behavior was observed with the mercury derivatives. Owing to the extremely low solubility of these compounds, electrocrystallization experiments were conducted in dry DMF. With the small anions BF_4^-, ClO_4^-, and PF_6^- microcrystalline precipitates were obtained at the anode, which all contain mercury, as shown by microprobe analysis. Of particular note is the obtention of thin black needles when **1c** is electrocrystallized in the presence of tetrabutylammonium thiocyanate as electrolyte. Microprobe analysis shows the presence of mercury as well as a S/Hg ratio value between 9 and 10, consistent with the formation of a cation-radical salt of **1c** with the thiocyanate anion.

In conclusion, while the silicon derivatives appear to dissociate upon oxidation into their individual cation radicals, the mercuric compounds retain their integrity, which make them particularly attractive for the elaboration of new cation-radical salts. The phosphorus derivatives are under investigation, and preliminary results show that, despite having reversible cyclic voltammograms, these phosphines tend to be oxidized to the phosphine oxides, probably by reaction of the cation radical with traces of water.

Further work in these directions will concentrate on the optimization of the electrocrystallization conditions and the synthesis of phosphine oxides or sulfides from the now readily available tertiary phosphines as well as the preparation of more soluble mercury derivatives.

Experimental Section

General Comments. All reactions were carried out under dry argon. Diethyl ether was distilled from Na/Ph_2CO immediately before use. TTF, 3,4-dimethyltetrathiafulvalene (o-DMTTF), and trimethyltetrathiafulvalene (tMTTF) were prepared according to published procedures.[15] Melting points are uncorrected. Microanalyses were performed at the Institut de Chimie des Substances Naturelles (CNRS), Gif/Yvette, France. Electrochemical data were obtained by cyclic voltammetry using a PAR-273 potentiostat. NMR spectra were recorded on a JEOL 60-MHz spectrometer, and mass spectra were obtained by chemical ionization.

Bis(tetrathiafulvalenyl)mercury (1a). A solution of TTF (0.5 g, 2.45 mmol) in Et_2O (50 mL) is treated at −78 °C successively with diisopropylamine (0.35 mL, 2.5 mmol) and BuLi (2.5 M in hexanes, 1 mL). The yellow precipitate is stirred at −78 °C for 1 h and then treated with mercuric chloride (0.33 g, 1.2 mmol). **1a** precipitates immediately. The solution is warmed to 20 °C; the yellow precipitate is filtered, washed with Et_2O and H_2O, and dried under vacuum over P_2O_5. Attempted recrystallization from DMF produces extensive decomposition; therefore, the product was not further purified (0.6 g, 80%): mp 214 °C. Anal. Calcd for $C_{12}H_6HgS_8$: C, 23.74; H, 0.99; S, 42.20. Found: C, 23.52; H, 1.27; S, 40.62.

(27) (a) Chiang, T. C.; Reddoch, A. H.; Williams, D. F. *J. Chem. Phys.* **1971**, *54*, 2051. (b) Kathirgamanthan, P.; Mucklejohn, S. A.; Rosseinsky, D. R. *J. Chem. Soc., Chem. Commun.* **1979**, 86. (c) Enkelman, V.; Morra, B.; Wegner, G.; Heinze, J. *Chem. Phys.* **1982**, *66*, 303. (d) Engler, E. M.; Greene, R.; Haen, P.; Tomkiewicz, Y.; Mortensen, K.; Berendzen, J. *Mol. Cryst. Liq. Cryst.* **1982**, *79*, 15. (e) Pénicaud, A.; Batail, P.; Davidson, P.; Levelut, A.-M.; Coulon, C.; Perrin, C. *Chem. Mater.* **1990**, *2*, 117.

(28) Batail, P.; Livage, C.; Parkin, S. S. P.; Coulon, C.; Martin, J. D.; Canadell, E. *Angew. Chem., Int. Ed. Engl.* **1991**, *30*, 1498.

(29) Boubekeur, K. Thesis, Rennes, France, 1989.

(30) Scott, B. A.; La Placa, S. J.; Torrance, J. B.; Silverman, B. D.; Welber, B. *J. Am. Chem. Soc.* **1977**, *99*, 6631.

Bis(3′,4′-dimethyltetrathiafulvalen-3-yl)mercury (1b). When a solution of o-DMTTF (0.57 g, 2.45 mmol) of dry Et_2O at −70 °C is successively treated with $HN(iPr)_2$ (0.35 mL, 2.5 mmol) and BuLi (2.5 M in hexanes, 1 mL), a yellow precipitate slowly appears. After the mixture is stirred for 1 h, mercuric chloride (0.33 g, 1.2 mmol) is added, the solution is warmed to room temperature, and the precipitate is filtered and washed with H_2O, EtOH, and Et_2O. Recrystallization from DMF affords **1b** as microcrystalline yellow needles (0.67 g, 85%): mp 210–213 °C. Anal. Calcd for $C_{16}H_{14}HgS_8$: C, 28.98; H, 2.11; S, 38.64. Found: C, 29.42; H, 2.13; S, 37.17.

Bis(4,3′,4′-trimethyltetrathiafulvalen-3-yl)mercury (1c). When tMTTF (0.5 g, 2.03 mmol) is treated as above, one obtains **1c** as yellow plates from DMF: mp 236 °C. Anal. Calcd for $C_{18}H_{18}S_8Hg$: C, 31.28; H, 2.60; S, 37.07. Found: C, 31.69; H, 2.50; S, 37.51.

Dimethylbis(tetrathiafulvalenyl)silane (2a). A solution of TTF (1.2 g, 5.9 mmol) in Et_2O (100 mL) is treated at −78 °C successively with diisopropylamine (0.61 mL, 6 mmol) and BuLi (2.5 M in hexanes, 2.4 mL). The yellow precipitate is stirred at −78 °C for 1 h and then treated with dimethylsilyl dichloride (0.4 mL, 3 mmol) diluted with Et_2O (40 mL). The precipitate dissolves. After the usual workup, the toluene solution is filtered on silica gel and the product recrystallizes from cyclohexane: yield 0.25 g (71%); mp 142–144 °C. Anal. Calcd for $C_{14}H_{12}S_8Si$: C, 36.17; H, 2.60; S, 55.18. Found: C, 36.57; H, 2.86; S, 53.94. ^1H NMR ($CDCl_3$): δ_H 6.44 (s, 1H), 6.23 (s, 2H), 0.46 (s, 3H, Me–Si). MS-CI: *m/z* 465 (M^+).

Dimethylbis(3′,4′-dimethyltetrathiafulvalen-3-yl)silane (2b). An Et_2O solution of 3,4-dimethyltetrathiafulvalene (o-DMTTF; 0.70 g, 3 mmol) is treated as above at −70 °C successively with $(iPr)_2NH$ (0.42 mL, 3 mmol), BuLi (1.2 mL), and Me_2SiCl_2 (0.14 mL, 1.15 mmol). After the mixture is warmed to room temperature, the precipitated solid is filtered, washed once with Et_2O, dissolved in toluene, filtered on a short silica gel column, and recrystallized from CH_3CN: yield 170 mg (25%); mp 210–212 °C. Anal. Calcd for $C_{18}H_{20}S_8Si$: C, 41.50; H, 3.87; S, 49.25. Found: C, 41.23; H, 3.76; S, 49.46. ^1H NMR ($CDCl_3$): δ_H 6.43 (s, 2H), 1.90 (bs, 12H), 0.43 (s, 6H). MS-CI: *m/z* 521 (M^+), 233 (TTF^+).

Dimethylbis(4,3′,4-trimethyltetrathiafulvalen-3-yl)silane (2c). As above, from trimethyltetrathiafulvalene (tMTTF; 0.5 g, 2 mmol), one obtains **2c** as yellow crystals from CH_3CN: mp 204–210 °C. Anal. Calcd for $C_{20}H_{24}S_8Si$: C, 43.75; H, 4.40; S, 46.72. Found: C, 43.17; H, 4.18; S, 46.79. ^1H NMR ($CDCl_3$): δ_H 2.0 (s, 6H, Me-TTF), 1.87 (s, 12H, Me_2-TTF), 0.42 (s, 6H, Me-Si). MS-CI: *m/z* 549 (M^+).

Bis(tetrathiafulvalenyl)phenylphosphine (3a). See ref 12.

Bis(3′,4′-dimethyltetrathiafulvalen-3-yl)phenylphosphine (3b). From o-DMTTF (1.86 g, 8 mmol), $HN(iPr)_2$ (1.12 mL, 8 mmol), and BuLi (1.6 M in hexanes, 5 mL, 8 mmol), one obtains a yellow precipitate of o-DMTTF-Li, which is further treated at −70 °C with dichlorophenylphosphine (0.5 mL, 3.5 mmol) dissolved in dry Et_2O. After the mixture is warmed to room temperature, the red precipitate is filtered, washed with Et_2O, and Sohxlet-extracted with toluene. Evaporation and recrystallization from toluene yields large orange crystals of **3b** (1.2 g, 60%): mp 197–199 °C. Anal. Calcd for $C_{22}H_{19}PS_8$: C, 46.28; H, 3.35; P, 5.42; S, 44.93. Found: C, 46.56; H, 3.31; P, 5.50; S, 44.78. ^1H NMR ($CDCl_3$): δ_H 7.40 (m, 5H, Ph), 6.67 (d, J = 9 Hz, C-H), 1.93 (s, 12H, Me). ^{31}P NMR ($CDCl_3$): δ_P −23.2. MS-CI: *m/z* 571 (M^+, 100), 341 (o-DMTTF-PPh^+), 233 (o-$DMTTF^+$).

Bis(4,3′,4′-trimethyltetrathiafulvalen-3-yl)phenylphosphine (3c). From tMTTF (1 g, 4 mmol), iPr_2NH (0.57 mL, 4 mmol), BuLi (1.6 mL), and Cl_2PPh (0.2 mL, 1.5 mmol), one obtains a yellow precipitate which is treated as above: yield 0.6 g (68%); mp 216–220 °C. Anal. Calcd for $C_{24}H_{23}PS_8$: C, 48.12; H, 3.87, S, 42.83; P, 5.17. Found: C, 47.81; H, 3.87; S, 40.18; P, 6.64. ^1H NMR ($CDCl_3$): δ_H 7.30 (s, 5H, Ph), 2.20 (s, 6H, Me), 1.87 (s, 12H, Me). ^{31}P NMR ($CDCl_3$): δ_P −40.2. MS-CI: *m/z* 599 (M^+), 247 ($tMTTF^+$).

Table VI. Crystal Data and Data Collection for 2a

formula (mol wt)	$C_{14}H_{12}S_8Si$ (464.85)
a (Å)	12.584(1)
b (Å)	24.96(1)
c (Å)	6.404(1)
V (Å^3)	2011(1)
Z	4
ρ_{calc} (g cm^{-3})	1.537
radiation	Mo Kα (λ = 0.710 69 Å) graphite monochromated
temp (K)	293 ± 1
cryst syst, space group	orthorhombic, *Pnma*
cryst dimens (mm)	0.36 × 0.15 × 0.06
μ (cm^{-1})	9.082
diffractometer	Enraf-Nonius CAD4-F
data collcd	$1 \le \theta \le 26°$; −h, +h; 0, k; 0, l
scan type; ω-scan width	$\omega/2\theta$; 0.7 + 0.35 tan θ
no. of rflns collcd	4735
no. of unique reflns	2477
no. of unique reflns used	808 [$I > 3\sigma(I)$]
R, R_w, GOF	0.034, 0.046, 1.01
max resid electron density, e Å^{-3}	0.22

TCNQ Salts of 1a and 1b. Adding 1 equiv of TCNQ to a solution of **1a** (**1b**) in DMF leads to the precipitation of a dark green precipitate, which is further filtered and washed successively with DMF, EtOH, and Et_2O. The exact stoichiometry of the charge-transfer salts, which cannot be recrystallized, could, in principle, be deduced from the microanalysis results. Both compounds differ slightly from an exact 1:1 ratio, but a 1:2 ratio can be excluded. Anal. Calcd for **1a**·TCNQ·2DMF ($C_{30}H_{24}S_8N_6O_2Hg$): C, 37.63; H, 2.53; N, 8.78; S, 26.78. Found: C, 37.76; H, 1.38; N, 8.61; S, 26.50. Calcd for **1b**·TCNQ ($C_{28}H_{16}S_8N_4Hg$): C, 38.85; H, 1.86; N, 6.47; S, 29.64. Found: C, 38.46; H, 2.22; N, 6.09; S, 27.44.

Electrochemical Measurements. Cyclic voltammograms were recorded with Pt working and auxiliary electrodes, an SCE reference electrode, and $Bu_4N^+PF_6^-$ as supporting electrolyte in CH_2Cl_2 unless otherwise stated. A ferrocene internal standard ($Fc^{+/0}$ couple) was measured after each experiment, and data were corrected for the $Fc^{+/0}$ couple at 0.39 V vs the SCE reference.

X-ray Structure Resolution of $(TTF)_2SiMe_2$ (2a). Accurate values of the unit cell parameters were determined from a least-squares treatment of the angular settings of 25 carefully centered reflections. The experimental details of the data collection and the least-squares refinement results are given in Table VI. The structure was solved by direct methods and refined (full-matrix least squares) anisotropically, with hydrogen atoms (at calculated ideal positions) included in structure factor calculations and not refined; a non-Poisson contribution weighting scheme was applied. Scattering factors are from ref 31, and the calculations were performed with the Enraf-Nonius SDP programs.[32]

Acknowledgment. This work was supported by the European Community Esprit Basic Research Action MOLCOM (No. 3121). We thank Drs. P. Batail and E. Canadell for numerous fruitful discussions.

Supplementary Material Available: Tables of positional and thermal parameters for all atoms, including hydrogen atoms (4 pages). Ordering information is given on any current masthead page.

OM920578K

(31) *International Tables for X-Ray Crystallography*; Kynoch Press: Birmingham, England, 1974.
(32) Frenz, B. A. *Computing in Crystallography*; Delft University Press: Delft, The Netherlands, 1978.